Electrosynthesis of Pd Single-Crystal Nanothorns and Their Application in the Oxidation of Formic Acid

Hui Meng,*,† Shuhui Sun,† Jean-Philippe Masse,‡ and Jean-Pol Dodelet*,†

INRS Énergie, Matériaux et Télécommunications, 1650 Boulevard Lionel Boulet, Varennes, Québec, Canada J3X 1S2, and (CM)2, École Polytechnique de Montréal, 2500 Chemin de Polytechnique, Montréal, Québec, Canada H3T 1J4

Received May 27, 2008. Revised Manuscript Received August 15, 2008

With a square wave electrochemical reduction method, Pd single-crystal nanothorns (Pd NTs) are prepared at room temperature, without template or surfactant. By varying the potentials applied, we can control the length and accumulation state of the Pd NTs. TEM study shows that the growth of the thorn occurs along the $(2\bar{2}0)$ plane. The nanothorn is made by a succession of epitaxic dodecahedrons of decreasing sizes aligned in the direction of the (111) plane. The surface chemical state of the Pd NTs is studied with XPS. Pd NTs have higher catalytic activity than commercial Pd black for the oxidation of formic acid.

Introduction

Palladium is one of the most used noble metals having technical applications in autocatalysts, dentistry, chemistry, and in the electronic industry.[1] It is also one of the main electrocatalysts used to perform the oxidation of formic acid in direct formic acid fuel cells (DFAFCs),[2−6] which are contemplated along with direct methanol and ethanol fuel cells for the fast expanding market of portable electrochemical power sources aimed at replacing batteries in the near future.[7]

Palladium is the electrocatalyst of choice in DFAFCs because, unlike Pt, it oxidizes formic acid to CO_2 without producing the metal poisoning CO intermediate.[8−10] So far, all studies about the use of Pd as an electrocatalyst for the oxidation of formic acid have dealt with Pd nanoparticles.[3] However, it is known that physical, chemical, and electrochemical properties of nanomaterials are strongly influenced by the morphology of the nanocrystals.[11,12] Various synthetic paths like template synthesis,[13,14] vapor deposition,[15−17] and colloidal synthesis[18,19] have indeed been explored to get different material architectures. In the case of Pd, for instance, the most frequent procedure to obtain nanostructures other than nanoparticles, is to prepare the new nanostructures with a template.[20] In this case, the template has to be removed and the resulting material is often polycrystalline. Only a few attempts have led to the preparation of single Pd nanocrystals without a template.[21−24]

In this work, we report on the electrochemical preparation of Pd single-crystal nanothorns (Pd NTs) obtained at room temperature, without template or surfactant. The diversity of electrodeposition parameters may lead to a great variety of nanoarchitectures, as has already been shown for other structures prepared electrochemically, like tetrahexahedral Pt nanocrystals,[12] nanotubes,[25] nanowires,[26,27] and meso-

* Corresponding author. E-mail: dodelet@emt.inrs.ca (J.-P.D.); meng@emt.inrs.ca. (H.M.).
† INRS Énergie, Matériaux et Télécommunications.
‡ (CM)2, École Polytechnique de Montréal.

(1) *Platinum 2007 Interim Review*; Johnson Matthey: London, 2007; http://www.platinum.matthey.com/uploaded_files/Int2007/full_int_07.pdf.
(2) Rice, C.; Ha, S.; Masel, R. I.; Waszczuk, P.; Wieckowski, A.; Barnard, T. *J. Power Sources* **2002**, *111*, 83.
(3) Ha, S.; Larsen, R.; Zhu, Y.; Masel, R. I. *Fuel Cells* **2004**, *4*, 337.
(4) Zhu, Y.; Khan, Z.; Masel, R. I. *J. Power Sources* **2005**, *139*, 15.
(5) Ha, S.; Larsen, R.; Masel, R. I. *J. Power Sources* **2005**, *144*, 28.
(6) Ha, S.; Dunbar, Z.; Masel, R. I. *J. Power Sources* **2006**, *158*, 129.
(7) Crawley, G. *2006 Portable Survey*; Fuel Cell Today: Hertfordshire, U.K., December 2006; http://www.fuelcelltoday.com/media/pdf/surveys/2006-Portable.pdf.
(8) Arenz, M.; Stamenkovic, V.; Schmidt, T. J.; Wandelt, K. P.; Ross, N.; Markovic, N. M. *Phys. Chem. Chem. Phys.* **2003**, *5*, 4242.
(9) Hoshi, N.; Kida, K.; Nakamura, M.; Nakada, M.; Osada, K. *J. Phys. Chem. B* **2006**, *110*, 12480.
(10) Zhou, W. P.; Lewera, A.; Larsen, R.; Masel, R. I.; Bagus, P. S.; Wieckowski, A. *J. Phys. Chem. B* **2006**, *110*, 13393.
(11) Xia, Y.; Yang, P.; Sun, Y.; Wu, Y.; Mayers, B.; Gates, B.; Yin, Y.; Kim, F.; Yan, H. *Adv. Mater.* **2003**, *15*, 353.
(12) Tian, N.; Zhou, Z. Y.; Sun, S. G.; Ding, Y.; Wang, Z. L. *Science* **2007**, *316*, 732.
(13) Pai, R. A.; Humayun, R.; Schulberg, M. T.; Sengupt, A.; Sun, J. N.; Watkins, J. J. *Science* **2004**, *303*, 507.
(14) Thurn-Albrecht, T.; Schotter, J.; Kästle, G. A.; Emley, N.; Shibauchi, T.; Krusin-Elbaum, L.; Guarini, K.; Black, C. T.; Tuominen, M. T.; Russell, T. P. *Science* **2000**, *290*, 2126.
(15) Hausmann, D.; Becker, J.; Wang, S. L.; Gordon, R. G. *Science* **2002**, *298*, 402.
(16) Li, Y. L.; Kinloch, I. A.; Windle, A. H. *Science* **2004**, *304*, 276.
(17) Gudiksen, M. S.; Lauhon, L. J.; Wang, J. F.; Smith, D. C.; Lieber, C. M. *Nature* **2002**, *415*, 617.
(18) Shevchenko, E. V.; Talapin, D. V.; Rogach, A. L.; Kornowski, A.; Haase, M.; Weller, H. *J. Am. Chem. Soc.* **2002**, *124*, 13958.
(19) Sun, Y.; Xia, Y. *Science* **2002**, *298*, 2176.
(20) Xu, C. W.; Wang, H.; Shen, P. K.; Jiang, S. P. *Adv. Mater.* **2007**, *19*, 4256.
(21) Xiong, Y.; McLellan, J. M.; Chen, J.; Yin, Y.; Li, Z. Y.; Xia, Y. *J. Am. Chem. Soc.* **2005**, *127*, 17118.
(22) Xiong, Y.; Cai, H.; Wiley, B. J.; Wang, J.; Kim, M. J.; Xia, Y. *J. Am. Chem. Soc.* **2007**, *129*, 3665.
(23) Xiong, Y.; Xia, Y. *Adv. Mater.* **2007**, *19*, 3385.
(24) Zhou, P.; Dai, Z.; Fang, M.; Huang, X.; Bao, J. J. *Phys. Chem. C* **2007**, *111*, 12609.
(25) Sander, M. S.; Gao, H. *J. Am. Chem. Soc.* **2005**, *127*, 12158.
(26) Xiao, Z. L.; Han, C. Y.; Kwok, W. K.; Wang, H. H.; Welp, U.; Wang, J.; Crabtree, G. W. *J. Am. Chem. Soc.* **2004**, *126*, 2316.
(27) Favier, F.; Walter, E. C.; Zach, M. P.; Benter, T.; Penner, R. M. *Science* **2001**, *293*, 2227.

10.1021/cm8014513 CCC: $40.75
Published on Web 10/29/2008

structures.[28] In this study, it will be shown that Pd NTs are prepared by potential square wave electrodeposition (a nucleation step, followed by a growth step). The length of the Pd NTs and their number per unit surface area of substrate can be controlled by adjusting the electronucleation potential. It will also be shown that these Pd NT architectures provide better performance toward formic acid electrooxidation than commercial Pd black.

Experimental Section

K_2PdCl_6 (99% purity), formic acid (98% purity), Nafion perfluorinated ion-exchange resin (5 wt % solution in lower aliphatic alcohols/H_2O mixture) and palladium black were purchased form Sigma-Aldrich. H_2SO_4 (95−98% purity) was purchased from Fisher Scientific. All the reagents were used as received. Graphite rods with a diameter of 0.6 cm were purchased from Poco Graphite, Inc. The graphite rods were cut into the size of electrodes (about 1.5 cm long). Their sections were polished by a succession of sand papers and polishing cloth on a polishing machine then finally ultrasonically cleaned. The cylindrical surface of the graphite rods was painted with an insulating varnish leaving their polished sections as working electrodes.

The morphology and structure of the Pd NTs were characterized by field emission scanning electron microscopy (FESEM, JEOL JSM7401F, operating at 15 kV), and by transmission electron microscopy (TEM, JEOL 2100F, operating at 200 kV). The as-prepared sample was observed with SEM without any treatment. For TEM observations, the surface layer of the graphite rod section was scratched to obtain powders that were mixed ultrasonically with methanol. Finally, a drop of the suspension was placed on a carbon film-coated copper grid, followed by solvent evaporation under ambient conditions. X-ray photoelectron spectroscopic (XPS) analysis was carried out in a VG ESCALAB 220iXL, using monochromated Al Kα source (1486.6 eV), at a based pressure of 2×10^{-9} mbar. High-resolution spectra were obtained at a perpendicular takeoff angle, using a pass energy of 20 eV and steps of 0.05 eV. All the binding energies were calibrated by placing the C1s line of adventitious hydrocarbon at 284.8 eV. After Shirley background removal, the component peaks were separated using the CasaXPS program. To reach to the inner layers of Pd NTs, etching was also performed in situ. The energy of etching ions was 3 KeV; the etched surface area, 1.5 mm × 2 mm; the vacuum pressure in the analysis chamber, 2×10^{-8} mbar; the etching rate, 2 nm/min; and the etching time was 5 min.

The electrochemical synthesis of Pd NTs, as well as their electrochemical and electrocatalytic characterizations, were all performed at room temperature with a 273A EGG Potentiostat and in the same standard three-electrode cell. A Pt mesh served as the counter electrode, with a saturated calomel electrode (SCE) as the reference. A 2 mM K_2PtCl_6 solution in 0.5 M H_2SO_4 was used for the electrosynthesis of Pd NTs, whereas the electrocatalytic properties of Pd NTs and commercial Pd black were measured after 10 cycles at 50 mV s^{-1} in a 0.2 M formic acid solution in 0.1 M H_2SO_4. No change in the cyclic voltammograms was observed between 10 and 30 cycles. All solutions were prepared using ultrapure water from a Barnstead Nanopure water system. The working electrode with Pd NTs was obtained directly from the electrosynthesis procedure. The working electrode with commercial Pd black was prepared as follows: 3.0 mg of Pd black was mixed with 2 mL of ultrapure water and sonicated for 30 min. An aliquot of 10 μL of the suspension was dropped onto the surface of the graphite rod and let to dry under ambient conditions. Finally, 10 μL of a 0.05 wt % Nafion solution was added to the catalyst layer. The amount of Pd on the surface of the electrode was 15 μg.

The electroactive surface areas of the Pd NTs and of Pd black were determined electrochemically by CO poisoning the metal followed by CO stripping (see the Supporting Information, Figure S7) The following steps were performed: (i) N_2 was bubbled into the 0.1 M H_2SO_4 solution for 60 min; (ii) CO was bubbled for 30 min while keeping the potential at −0.14V vs SCE for CO poisoning; (iii) N_2 was bubbled vigorously to remove traces of dissolved CO; (iv) cyclic voltammetry was performed at a scan rate of 50 mV s^{-1} and from −0.14 to 1.0 V vs SCE for the CO poisoning, and −0.24 to 1.0 V vs SCE for the second cycle. The CO surface area S_{CO} in cm^2 was determined as follows[29]

$$S_{CO} = \frac{Q_{CO}}{0.420 \text{ mC cm}^{-2}}$$

where Q_{CO} is the CO stripping charge (in mC) determined after 30 min of CO adsorption, and 0.420 mC cm^{-2} corresponds to a monolayer of adsorbed CO. The surface areas calculated from CO poisoning and stripping are 1.925 cm^2 for the Pd black and 0.197 cm^2 for the Pd NTs.

Results and Discussion

The Pd nanothorns presented in Figure 1a, b, and c are all obtained by electrochemical reduction of a 2 mM K_2PdCl_6 solution in 0.5 M H_2SO_4. The NT electrosynthesis proceeds in two steps: (i) a square wave nucleation and (ii) a square wave growth of the NTs. In the nucleation step, the working electrode, which is the section of a graphite rod, is first maintained at 0.8 V vs SCE for 50 ms. This is followed by a 20 ms step at a reducing potential varying from 0 to −1.0 V vs SCE. This nucleation cycle is performed 600 times. It is followed by a growth cycle during which the potential of the working electrode is scanned every 5 ms between 0.6 and 0.25 V vs SCE. This growth cycle is performed 180 000 times. The two reduction reactions involved in these experiments are

$$PdCl_6^{2-} + 2e^- \rightarrow PdCl_4^{2-} + 2Cl^- \quad E^0 = 1.29 \text{ V (NHE) or } 1.05 \text{ V (SCE)} \quad (1)$$

$$PdCl_4^{2-} + 2e^- \rightarrow Pd + 4Cl^- \quad E^0 = 0.623 \text{ V (NHE) or } 0.382 \text{ V (SCE)} \quad (2)$$

Pd nanostructures obtained by electrosynthesis using three different nucleation potentials are shown in Figure 1a−c. The latter figures display mostly Pd NTs. A sequence of Pd NTs obtained at reduction potentials ranging from 0 to −1.0 V vs SCE is disclosed in Figure S1 of the Supporting Information. By analyzing Figures 1 and S1, one may conclude that the length and the density of NTs per unit surface area substrate vary with the nucleation potential. The change of the NT length with the applied nucleation potential is presented in Figure 1d. This curve shows a first plateau around 250 nm for potentials down to −0.5 V vs SCE. It is followed by a second plateau around a NT length of 650 nm for more negative nucleation potentials. As the diameter

(28) Subhramannia, M.; Ramaiyan, K.; Pillai, V. K. *Langmuir* **2008**, *24*, 3576.

(29) Vidakovic, T.; Christov, M.; Sundmacher, K. *Electrochim. Acta* **2007**, *52*, 5606.

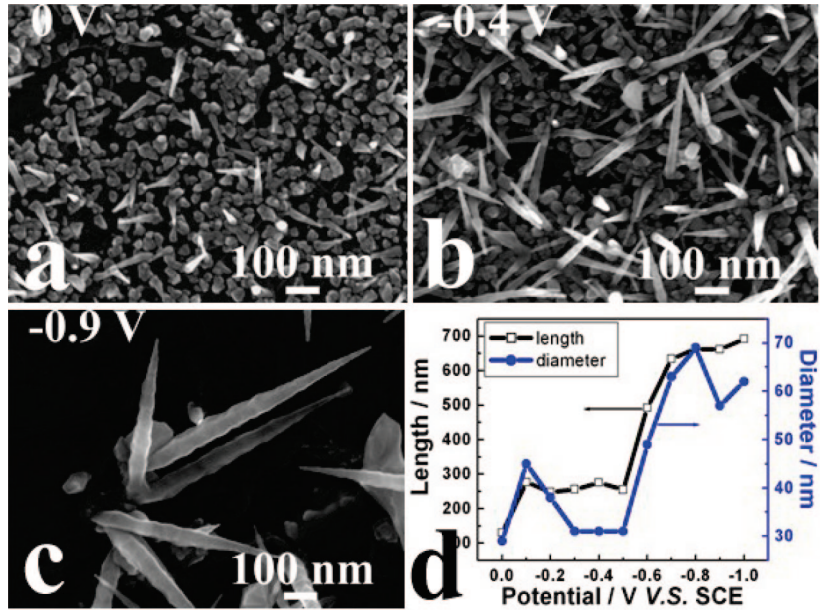

Figure 1. SEM images of Pd nanothorns obtained after nucleation at (a) 0, (b) −0.4, and (c) −0.9 V vs SCE; (d) length and diameter of the Pd nanothorns vs nucleation potential.

of the thorns is changing along their length, it was decided to characterize the thorn diameter by the diameter of its basis. As shown in Figure 1d, the diameter of the thorn also varies with the potential according to a trend similar to that of the thorn's length. The density of NTs per unit surface area is more difficult to quantify, but according to the sequence of SEM pictures presented at low and high magnifications in Figure S1 of the Supporting Information, the density of NTs per unit area increases, goes through a maximum, and then decreases as the nucleation potential goes from 0 to −1.0 V vs SCE. The maximum density seems to be obtained at −0.4 ± 0.1 V vs SCE. A last conclusion reached after observing Figures 1 and S1 is that, in the low potential region (down to about −0.5 to −0.6 V vs SCE), Pd NTs are mostly individual structures. For more negative potentials, several NTs seem to have a common or a joint basis. This potential range also corresponds to the potentials where longer Pd NTs are found. The origin of multiple Pd NT growth is, however, not multiple Pd NT seeds, as those are seen at all nucleation potentials on SEM micrographs recorded directly after the nucleation step (Figure S2 in the Supporting Information).

Most of the nanostructures seen in Figures 1 and S1 are Pd NTs. Occasionally, however, other Pd nanostructures appeared like the ones seen in Figure S3 of the Supporting Information. Here the electroreduction step was performed at −0.15V vs SCE. One of the nanostructures appearing in Figure S3 of the Supporting Informtation enabled us to understand how Pd NTs are formed. The latter nanostructure is also presented in Figure 2a. From this figure, it is clear that a dodecahedron (a volume limited by 12 pentagonal faces) is at the basis of the NT (Figure 2b). It is proposed that the nanothorn is developed by the growth, on only one face of the dodecahedron, of a succession of epitaxic dodecahedrons of decreasing sizes, alike what is drawn in Figure 2c. Going back to Figure S3 in the Supporting Information, it seems that all Pd NTs have a dodecahedron at their basis. Furthermore, among all the other Pd nanostructures recognized in Figure S3 in the Supporting Information (several cubes, one octahedron, etc.), none of them developed nanothorns. It is to be noted that the sharp angles seen on the Pd NT drawn in Figure 2c are attenuated on the actual NTs seen in Figures 1, 1S, or 2a. This is mainly due to the fact that the growth step involves a succession of oxidation and reduction steps of Pd (reaction 2), a process that will smear the sharp angles and produce a NT with a more monolithic shape.

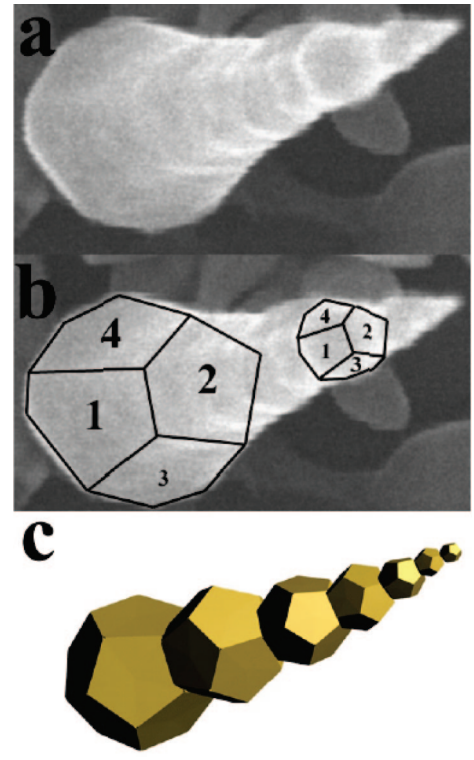

Figure 2. SEM image of (a) a Pd nanothorn, (b) the same Pd nanothorn showing its dodecahedron basis, (c) a representation of the nanothorn with its sequence of epitaxic dodecahedrons of decreasing volumes as a model for the actual Pd nanothorn shown in (a).

Figure 3. TEM micrograph showing two Pd nanothorns.

One may wonder what happens when the parameters of the square wave electrosynthesis of NTs are modified or when the electrosynthesis is attempted with triangular waves or even in potentiostatic conditions. To answer these questions, experiments were first performed in square wave conditions by doubling or halving: (i) the total time of step 1 (using 1200 cycles for doubling); (ii) the width of step 1 (using 100 ms at 0.8V and 40 ms at potentials comprised between 0 and −1.0 V, for doubling); (iii) the total time of step 2 (using 360 000 cycles for doubling); and (iv) the width of step 2 (using 10 ms at 0.6 V and 10 ms at 0.25 V for doubling). All these changes produce nanothorns similar to those previously described. Changes are only seen in the size and the surface density of the NTs. Pure Pd nanothorns (no visible Pd particles) may even be obtained when 600 cycles of step 1 (0.8 V, 50 ms / −0.6 V, 20 ms) are followed by 360 000 cycles of step 2 (0.6 V, 5 ms / 0.25 V, 5 ms) as seen in Figure S4 in the Supporting Information. When a triangular wave is applied at the same frequency and between the same potential limits than for the square wave, only short and thick nanothorns are obtained (Figure S5 in the Supporting Information). No nanothorns are obtained in potentiostatic conditions. From these results, it was concluded that the abruptness of the potential step, which is characteristic of a square wave, is a requirement to obtain NTs as much larger currents are feeding the nuclei in these conditions than for a triangular potential wave or even in potentiostatic conditions.

To get more insight into the structure of the Pd NTs, we also examined them by TEM and HRTEM. Figure 3 is a TEM micrograph showing two NTs obtained after an electroreduction step at −0.7 V vs SCE. As the SEM pictures

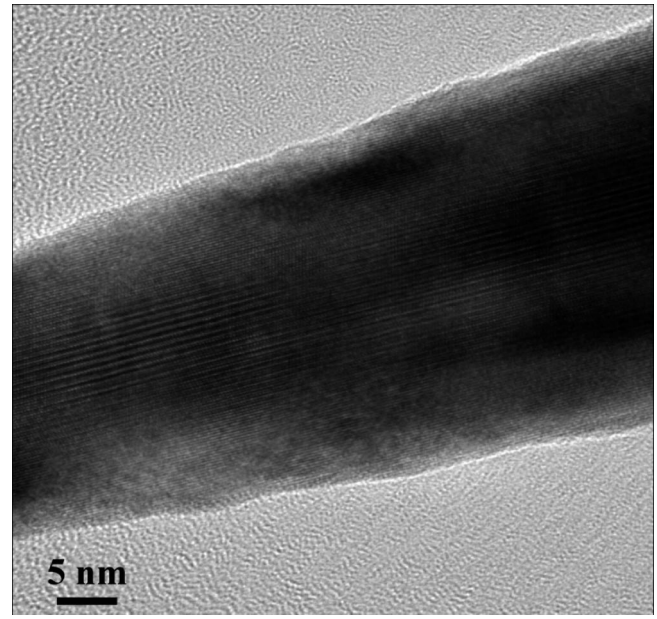

Figure 4. High-resolution TEM micrograph of a section of Pd nanothorn.

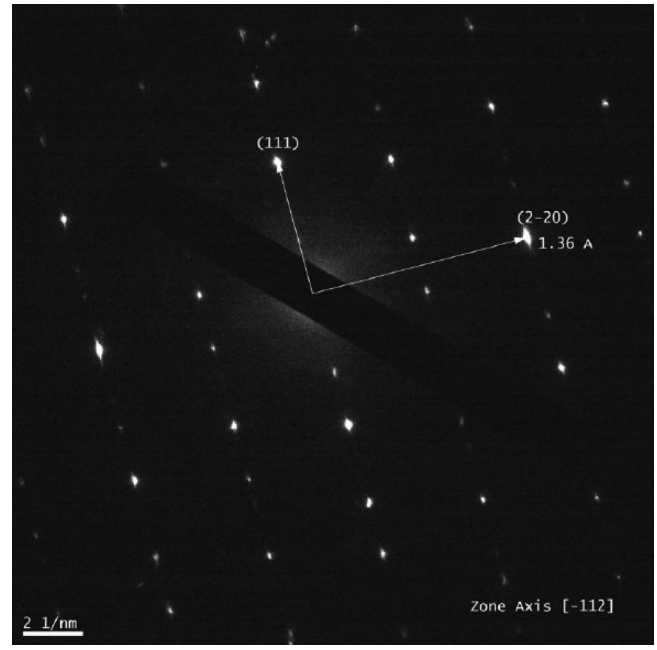

Figure 5. Selected area electron diffraction of a region of Figure 4.

of Figures 1 and 2, the TEM micrograph also shows that the NT is made in sequence with epitaxic units being smaller and smaller from the basis to the tip of the nanothorn. Figure 4 shows a HRTEM micrograph of a fraction of a nanothorn displaying well resolved continuous fringes having the same orientation. It is possible to follow these fringes from the basis to the tip of the NT, revealing therefore its single crystal epitaxial character. The main fringes lying parallel to the NT long axis are (111) planes with fringe spacings of 0.223 nm typical of fcc Pd. Figure 5 shows the selected area electron diffraction (SAED) of a region of Figure 4. Two sets of spots can be identified. They are (111) and $(2\bar{2}0)$ with a d spacing of 0.223 and 0.136 nm, respectively. Figure 5 indicates that if the main axis of the NT is along the (111) plane, the growth of the thorn occurs along the $(2\bar{2}0)$ plane,

which is perpendicular to the (111) plane. A further proof of the single-crystal character of the NTs is given by sonicating them, as no breaking apart of individual dodecahedrons was ever seen in these conditions. Darker regions seen in Figures 3 and 4 are believed to be produced by structural defects in the single crystal.

The metallic character of the Pd NTs has also been probed by X-ray photoelectron spectroscopy. XPS results revealed an oxide layer on the surface of the Pd NTs. To get the information of the inner layer of the NTs, etching with Ar ions was performed in the analysis chamber of the XPS. The Pd3d narrow scan spectra of the NTs, before and after etching the nanothorns are displayed in Figure S6 of the Supporting Information. The spectrum recorded after etching shows only two asymmetric Pd peaks assigned to $Pd_{5/2}$ and $Pd_{3/2}$ having a binding energy of 335.1 and 340.4 eV, typical of Pd metal,[14] whereas two other peaks, typical of palladium oxide,[30] appear at 338.1 and 343.0 eV on the spectrum before etching. This means that the very surfaces of the metallic Pd NTs are covered with a thin (<10 nm) layer of oxide.

Many studies have been performed on the oxidation of formic acid by Pd particles.[31−33] Here, the oxidation of formic acid is conducted on Pd NTs in order to evaluate their catalytic properties and compare them to those of commercial Pd black. This is shown in Figure 6. The NTs obtained by nucleation at −0.7 V vs SCE were used for this measurement. The currents have been normalized to 1 cm^2 of electroactive surface area for Pd NTs or Pd black. The latter has been measured by cyclic voltammetry after CO poisoning and stripping (see Figure S7). In Figure 6, when the potential increases from −0.2 to 1.0V vs SCE, the first oxidation peak observed on Pd NTs at 0.033V is assigned to the oxidation of HCOOH and the minor hump at about 0.5V is due to Pd oxidation. On the return trip, the peak around 0.45 V is the reduction of Pd oxide, followed at more negative potentials by the oxidation of HCOOH on newly reduced Pd surfaces. For the Pd black all is the same except that the oxidation peak of HCOOH in the positive direction appears at 0.143V. The better catalytic activity of Pd NTs vs that of Pd black, which is inferred from its smaller oxidation potential, is also confirmed by the much larger 3-fold oxidation current obtained for the NTs (∼ 6 mA cm^{-2}) compared with that of Pd black (∼2 mA cm^{-2}). Work is now in progress to generate large amounts of small Pd NTs in order to be able to try them as the anode in DFAFC.

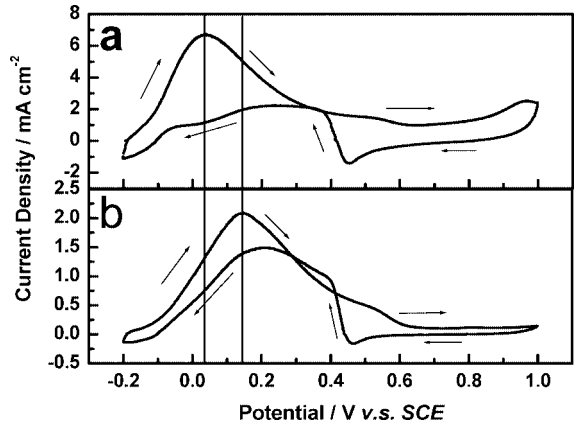

Figure 6. Electrocatalytic activities for the oxidation of formic acid for (a) Pd nanothorns and (b) Pd black. The sweep rate is 50 mV/s and the curves are the final ones after 10 circles, once the voltammograms became superposable.

Conclusions

In summary, Pd single-crystal nanothorns were prepared electrochemically in ambient conditions without using template or surfactant. By varying the potential during the nucleation step, it is possible to control the length and the density of the NTs per unit surface area of electrode. The novel structure is made by sequential epitaxy of dodecahedrons of decreasing volume aligned in a single direction, that of the (111) plane. This structure is strongly catalytic for the electro-oxidation of formic acid, the reaction occurring at the anode of direct formic acid fuel cells.

Acknowledgment. The authors thank the Natural Sciences and Engineering Research Council of Canada for funding.

Supporting Information Available: SEM of Pd nanothorns at different potentials, Pd after electronucleation, Pd nanostructures of various shapes, pure Pd nanostructures, Pd nanostructures obtained with triangular potential waves, Pd XPS spectra, and determination of the surface area of the Pd nanothorns (PDF). This material is available free of charge via the Internet at http://pubs.acs.org.

CM8014513

(30) Moulder, J. F.; Stickle, W. F.; Sobol, P. E.; Bomben, K. D. *Handbook of X-ray Photoelectron Spectroscopy*; Chastain, J., Ed.; Perkin-Elmer Corporation Physical Electronics Division: Eden Prairie, MN, 1992.
(31) Li, H.; Sun, G.; Jiang, Q.; Zhu, M.; Sun, S.; Xin, Q. *Electrochem. Commun.* **2007**, *9*, 1410.
(32) Bera, D.; Kuiry, S. C.; Seal, S. *J. Phys. Chem. B* **2004**, *108*, 556.
(33) Zhou, W.; Lee, J. Y. *Electrochem. Commun.* **2007**, *9*, 1725.